Measurements of the *K*-shell ionization cross sections of Si by 3–25-keV electron impact using the thick-target method

Jingjun Zhu (朱敬军), Zhu An (安竹),* Mantian Liu (刘慢天), and Lixia Tian (田丽霞)
Key Laboratory of Radiation Physics and Technology of Ministry of Education, Institute of Nuclear Science and Technology, Sichuan University, Chengdu 610064, People's Republic of China
(Received 6 April 2009; published 27 May 2009)

In this paper, the *K*-shell ionization cross sections of Si element in the threshold energy region of 3–25 keV have been measured by using the thick-target method. With the Monte Carlo simulations, the effects of multiple scattering of incident electrons and from the bremsstrahlung photons and other secondary particles in the thick-target method have been discussed. The detection efficiency calibration in the lower-energy region has been performed by using the bremsstrahlung spectra of thick carbon target by electron impact in combination with the use of standard x-ray sources, and the detector thickness parameters have also been determined by a nonlinear least-squares fit. The ill-posed inverse problem involved in the thick-target method has been dealt with by the Tikhonov regularization method. The experimental *K*-shell ionization cross sections for Si element obtained in this paper have also been compared with some theoretical models, and it has been observed that the experimental data in this paper are in good agreement with the theoretical values based on the distorted-wave Born approximation model developed most recently.

DOI: 10.1103/PhysRevA.79.052710 PACS number(s): 34.80.Dp, 02.30.Zz, 02.70.Uu

I. INTRODUCTION

Atomic inner-shell ionization cross sections by electron or positron are very important not only for better understanding electron or positron-atom interactions but also for a lot of applications in radiation physics, astrophysics, plasma physics, and electron or positron-matter interaction modeling, as well as in quantitative analysis (i.e., electron probe microanalysis, Auger electron spectroscopy, and electron energy loss spectroscopy) [1–5]. Especially, the atomic *K*-shell ionization cross sections by electron impact are recently needed in the studies of relativistic laser-matter interactions [6–8]. The atomic inner-shell ionization cross sections by electron impact have been measured for many years. In 2000, the experimental data available up to December 1999 for *K*-shell ionization by electron impact were compiled by our group [9]. In recent years, some groups have performed the measurements of atomic inner-shell ionization cross sections by electron impact [10–16], but, on the whole, the experimental information for atomic inner-shell ionization is still fairly limited [17]. For most elements, the experimental data for *K*-shell ionization are reported at a few electron incident energies and the experimental accuracies still need to be improved. For *L*-shell ionization, the experimental data are much less abundant although in recent years the measurements for *L*-shell ionization are increasing. For *M* shell, only very few experimental data have been reported [17]. Comparing with the experimental data of atomic inner-shell ionization by electron impact, the experimental data for positron impact are very scarce [3,4,18,19]. Therefore, more experimental data measured accurately for atomic inner-shell ionization by electron or positron impact are still largely needed.

Up to now, a number of theoretical model for atomic inner-shell ionization by electron or positron impact have been proposed based on various treatments of incident and outgoing wave functions, atomic structure and treatments of relativistic Coulomb and exchange effects, and so on. The early theoretical models have been reviewed by Powell [1,2]. Since then, the theoretical studies for atomic inner-shell ionization by electron and positron impact have been made great progress. For example, based on the plane-wave Born approximation (PWBA), Hippler [20] proposed a PWBA-C-Ex model which incorporated the exchange, Coulomb, and relativistic corrections and included the transverse interaction of virtual photons with atoms; Rez [21] reported the calculations for *K*, *L*, and *M* shells. Moreover, Kim and co-workers [22,23] extended the binary-encounter-dipole model to relativistic incident electron energies for calculating the *K*-shell ionization cross sections by electron impact; Uddin *et al.* [24,25] also employed the modified version of the improved binary-encounter-dipole model, which incorporated the ionic and relativistic effects, to calculate the *K*-shell ionization cross sections by electron impact. Within the framework of nonrelativistic perturbation theory, which takes into account the one-photon exchange, Mikhailov *et al.* [26,27] deduced the universal scaling behavior for *K*-shell ionization cross sections by electron and positron impact. Especially, most recently, Segui *et al.* [28] and Colgan *et al.* [29] developed a distorted-wave Born approximation (DWBA) to calculate the atomic inner-shell ionization cross sections by electron and positron impact, which consistently accounts for the effects of both exchange and distortion. By combining the relativistic PWBA with the semirelativistic DWBA, a model has been proposed very recently by Bote and Salvat [30], which enables theoretical calculations for atomic inner-shell ionization by electron and positron impact to be carried out up to arbitrarily high energies. Besides the theoretical models described above, a lot of empirical and semiempirical formulas have also been proposed for being easily used in the algorithms developed for the microanalysis and in some other applications [1,2]. In recent years, some new empirical and

*Corresponding author; FAX: +86 28 85410252; anzhu@scu.edu.cn

semiempirical formulas were also developed [31–35]. Among them, the empirical formulas of Casnati *et al.* [31] and Hombourger [32] are now widely used.

Most of experimental data for atomic inner-shell ionization by electron and positron impact are measured by using thin self-supporting samples or thin samples deposited on very thin substrates [9]. But, the preparations of thin self-supporting samples or thin samples deposited on very thin substrates are not easy [36]. In recent years, we developed a so-called thin sample on thick-substrate method to circumvent the difficulties of preparing thin self-supporting samples or thin samples on very thin substrates [13–15]. In this method, we take into account the effect of multiple scattering of incident electrons through thin samples, the effect of backscattering of incident electrons from substrates, and the effect of bremsstrahlung photons produced by incident electrons bombarding thick substrates [11,15]. In the meantime, the thickness values of the thin samples in all thin-sample methods have to be measured accurately to ensure the experimental accuracy [11,37]. A few techniques can be utilized to determine the thin-sample thickness, such as Rutherford backscattering spectrometry [11,37,38], but the thickness determination of thin sample is often one of the main error sources in the experiments. Therefore, most recently, we exploited a so-called thick-target method, in which both the preparation of thin sample and its thickness determination are not involved [39]. In our studies for the thick-target method, by using the Monte Carlo simulations, we discussed the effects of multiple scattering of incident electrons, bremsstrahlung photons, and other secondary particles [39], as well as the effect of target surface roughness [40]. Moreover, we also adopted the Tikhonov regularization and the classical molecular dynamics to successfully treat the ill-posed inverse problems involved in the thick-target method [41]. It has been concluded that the thick-target method can be reliably used in the measurements for atomic inner-shell ionization cross sections near the threshold energy region [41]. In the present paper, the thick-target method will be used to measure the atomic inner-shell ionization cross sections by electron impact.

As mentioned before, the DWBA theories, most recently developed by Segui *et al.* [28] and Colgan *et al.* [29], for calculating the atomic inner-shell ionization cross sections by electron and positron impact, can consistently account for the effects of both exchange and distortion. At present, the theoretical predictions based on the DWBA theories developed by Segui *et al.* [28] and Colgan *et al.* [29] are, on the whole, in very good agreement with the experimental data. But, these comparisons mainly focused on the *L*-shell experimental data for higher- and lower-*Z* elements and on the *K*-shell experimental data for medium-*Z* elements near the threshold energy region [15,28–30]. Therefore, in this paper, we will measure the atomic *K*-shell ionization cross sections by electron impact for a lower-*Z* element, i.e., Si element, by using the thick-target method, and compare the measured data for Si element with some theoretical values. The other reason for selecting Si element is that the measured *K*-shell ionization cross sections for Si element near the threshold energy region were available at only a few incident energies in a narrower energy region [9].

This paper is organized as follows. Section II introduces the thick-target method and discusses the effects of multiple scattering of incident electrons, bremsstrahlung photons, and other secondary particles for Si thick target by using the Monte Carlo simulations. Moreover, in Sec. II the detection efficiency calibration based on the thick carbon target bremsstrahlung spectrum is also introduced. In Sec. III, the experimental results for the *K*-shell ionization cross sections of Si element by the thick-target method and some discussions are presented. The conclusions are given in Sec. IV.

II. METHODS

A. Thick-target method

As stated in [39], if we ignore the multiple scattering of incident electrons, i.e., the incident electrons are assumed to move straight in the thick sample, and, moreover, ignore the contributions from the bremsstrahlung photons and other secondary particles, the characteristic x-ray yield N_X for atomic inner-shell ionization induced by incident electrons in a thick sample can be given as follows [39]:

$$\frac{N_X(E_0)}{I_0} = \frac{N_A}{A}\frac{\Omega}{4\pi}\varepsilon\int_0^{E_0}\sigma_X(E) \times \exp\left(-\mu_X\frac{\cos\alpha}{\cos\beta}\int_E^{E_0}\frac{dE^*}{S(E^*)}\right)\frac{dE}{S(E)}. \quad (1)$$

Here E_0 is the incident energy, I_0 is the number of incident electrons, N_A is the Avogadro constant, A is the atomic mass number, $\Omega\varepsilon/4\pi$ is the detection efficiency, σ_X is the characteristic x-ray production cross section, μ_X is the mass attenuation coefficient for characteristic x ray inside the sample, $S(E)=(-1/\rho)(dE/dX)$ is the mass stopping power, α is the incident angle, i.e., the angle between the incident direction and the target normal, and β is the angle between the x-ray detector direction and the target normal.

Equation (1) is a Fredholm integral equation of first kind and its solution is typically an ill-posed inverse problem [42,43], i.e., the solution, σ_X, is very sensitive to the perturbation of $N_X(E_0)/I_0$, which is inevitable because of the experimental statistics. Therefore, in [41], by using the Tikhonov regularization and the classical molecular dynamics, we have satisfactorily dealt with this ill-posed inverse problem. In this paper, we will use the Tikhonov regularization method in data processing. Here, we give a brief description for the Tikhonov regularization method [41], which is the most common and well-known form of regularization and widely used in many applications for dealing with ill-posed inverse problems. We can rewrite Eq. (1) as follows:

$$N(E_0) = \int_0^{E_0}\sigma_X(E)K(E,E_0)dE, \quad (2)$$

where

$$N(E_0) = \frac{N_X(E_0)}{I_0(E_0)}, \quad (3)$$

and when $E \leq E_0$,

$$K(E,E_0)=\left(\frac{N_A}{A}\frac{\Omega}{4\pi}\varepsilon\right)\exp\left(-\mu_X\frac{\cos\alpha}{\cos\beta}\int_E^{E_0}\frac{dE^*}{S(E^*)}\right)/S(E), \tag{4}$$

and when $E>E_0$, $K(E,E_0)=0$. If we have n experimental data at incident energies $E_{01},\ldots,E_{0n}$, the solutions for $\sigma_X(E)$ in Eq. (2) obtained with the Tikhonov regularization method are defined as the function $\sigma_X^{\lambda}(E)$, which minimizes the following quantity:

$$V(\lambda)=\sum_{i=1}^{n}\frac{1}{\sigma_i^2}\left(N(E_{0i})-\int_0^{E_0}\sigma_X(E)K(E,E_{0i})dE\right)^2+\lambda\|L\sigma_X\|_{L_2}^2. \tag{5}$$

Here, σ_i are the errors of $N(E_{0i})$, λ is the regularization parameter, L is an operator, which usually is identity or the second derivative, and the norm $\|\ \|_{L_2}$ is defined as follows for an arbitrary function f:

$$\|f\|_{L_2}^2=\int f^2(t)dt. \tag{6}$$

In the Tikhonov regularization method, the determination of the regularization parameter λ is very important for which many methods were proposed. In this paper, a so-called SC-method (SC for self-consistent), developed by Weese and co-workers [42,43], will be used.

B. Monte Carlo simulations in the thick-target method

As pointed out in Sec. II A, Eq. (1) is exactly valid only when it is assumed that the multiple scattering of incident electrons and the contributions from the bremsstrahlung photons and other secondary particles are ignored. In this section, we will use Monte Carlo simulations, in combination with the results of Eq. (1), to discuss the effects of multiple scattering of incident electrons and from the bremsstrahlung photons and other secondary particles.

The Monte Carlo code PENELOPE [44], which can allow the simulations of electron, positron, and photon transport in the energy range of 50 eV–1 GeV, is used in this paper. The PENELOPE code implements the most reliable cross sections and relaxation data available for the elements, and the physics models employed in this code also represent the state of the art for simulations of keV electron transport and x-ray generation [5]. Moreover, this code also includes a geometry package, which can flexibly perform the automatic tracking of particles in complex geometrical structures consisting of homogeneous bodies limited by quadric surfaces. The reliability and validity of the PENELOPE code have also been very well demonstrated [45–47].

For our Monte Carlo simulations in this paper, the incident electrons impact vertically, the x-ray detector is placed horizontally, and the thick Si target is tilted by 45° with respect to the direction of incident electron beams. This configuration for Monte Carlo simulations is the same as our experimental setup. Moreover, the half angle of the x-ray detector subtended to the center of the thick Si target is assumed to be 5°. In Fig. 1 the characteristic *K*-shell x-ray yields for Si element at several incident energies by using the Monte Carlo simulations are shown. Because the energies of characteristic $K\alpha$ and $K\beta$ x rays of Si element are very close, i.e., 1.74 and 1.84 keV and they cannot be separated in experimental x-ray energy spectra, therefore, the characteristic *K*-shell x-ray yields obtained by the Monte Carlo simulations include the characteristic $K\alpha$ and $K\beta$ x rays for Si element. Based on Eq. (1), the characteristic *K*-shell x-ray yields for Si element can also be calculated, and all atomic parameters involved in Eq. (1) are taken from the database of the PENELOPE code in order to compare the results both from Eq. (1) and from the Monte Carlo simulations. In Fig. 1, we can observe that the characteristic *K*-shell x-ray yields for Si element obtained by using Monte Carlo simulations and based on Eq. (1) are in excellent agreement in the energy region less than 26 keV. Therefore, in the case of the thick Si target, the multiple scattering of incident electrons and the contributions from the bremsstrahlung photons and other secondary particles can be indeed ignored in the energy region of interest here.

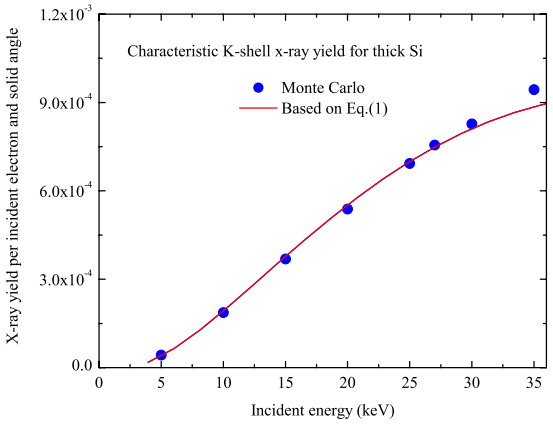

FIG. 1. (Color online) The characteristic *K*-shell x-ray yields for thick Si target by electron impact. The solid line represents the results based on Eq. (1) where the angles of α and β are 45°. The circles denote the results of Monte Carlo simulation.

C. Detection efficiency calibration

In general, the detection efficiency calibration for an x-ray detector can be performed by using standard x-ray sources, for example, ^{241}Am, ^{137}Cs, ^{55}Fe, ^{57}Co, and so on. Unfortunately, the standard x-ray source available in the energy region less than 3.3 keV for the detection efficiency calibration, which is very important for the measurements of atomic inner-shell ionization cross sections for elements (e.g., Si element) having low-energy characteristic x rays, is very rare. Therefore, in [48], we carried out the detection efficiency calibration in low-energy region by using the bremsstrahlung spectra of thick carbon target by electron impact, i.e., the shape of detection efficiency curve was determined from the ratio of experimental and theoretical bremsstrahlung spectra of thick carbon target by 19 keV electron impact, and the absolute values of detection efficiency curve were obtained from the use of ^{241}Am standard x-ray source. The choice of carbon as the target is because it has no char-

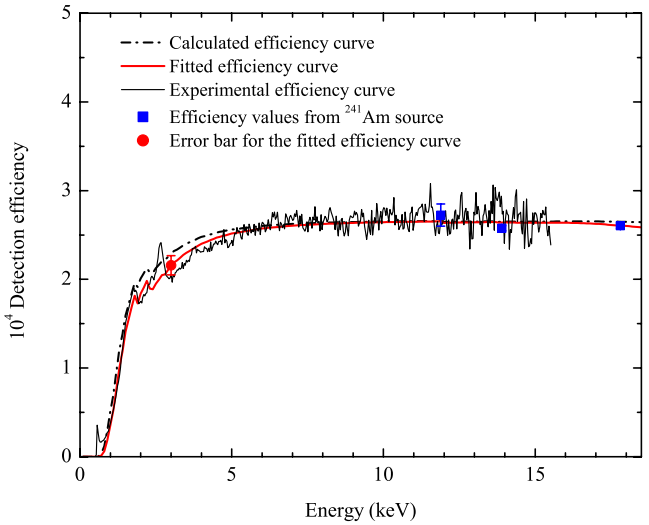

FIG. 2. (Color online) The x-ray detection efficiency of the Si(Li) detector. The calculated efficiency curve is based on the model of Eq. (7) and the thickness parameters given by the detector manufacturer. The fitted efficiency curve is obtained by fitting the experimental efficiency curve which is obtained from the ratio of experimental and theoretical bremsstrahlung spectra of thick carbon target by 19 keV electron impact and is normalized to the efficiency values obtained with the ^{241}Am standard x-ray source.

acteristic lines above 0.3 keV. In [48], the theoretical bremsstrahlung spectrum of thick carbon target by 19 keV electron impact was calculated by an analytic formula, i.e., the modified Wentzel's formula. At present, the Monte Carlo simulations for electron and photon transport have been made progress. The most reliable theoretical scaled differential cross sections [49,50] and shape functions [51] for bremsstrahlung have been incorporated into Monte Carlo simulations [5,45], and it has been shown that the experimental and theoretical bremsstrahlung spectra of thick targets by keV electron impact are in excellent agreement in the energy region where the intrinsic detection efficiency of x-ray detector is equal to 1 [5,45]. Therefore, in this paper, the method for detection efficiency calibration is still the same as in [48], but the theoretical bremsstrahlung spectrum is obtained by using the Monte Carlo PENELOPE code [52]. The simulation is totally the same as in Sec. II B, just with a thick carbon target instead of the thick Si target.

In Fig. 2, the shape of detection efficiency curve, obtained from the ratio of experimental and theoretical bremsstrahlung spectra of thick carbon target by 19 keV electron impact, is shown and it has been normalized to detection efficiency values obtained with ^{241}Am standard x-ray source. When the detection efficiency calibration is performed by using the standard x-ray sources, the standard sources are placed in the same position for mounting the Si target, and the effect of the thin polyethylene cover foil ($\sim$21.3 mg/cm^2) of the standard x-ray sources is also corrected. The standard x-ray sources used in this paper were provided by the Physikalisch-Technische Bundesanstalt (PTB), Germany and the accuracies of which are $\sim$1% (k=2). For all standard x-ray sources, their half-lives, x-ray energies, and emission probabilities are taken from the values most recently recommended by the International Atomic Energy Agency (IAEA) [53]. The accuracy of the detection efficiency calibration with the method described here is estimated to be $\sim$5%, which is mainly from the use of the standard x-ray sources [48,52].

The intrinsic detection efficiency versus x-ray energy can be expressed as follows [54,55]:

$$\varepsilon(E) = T(E)T_{col}(E)A(E), \tag{7}$$

where $T(E)$ represents the transmittance of the successive absorbing layers of x-ray detector (i.e., Be window, Au contact layer, and Si dead layer), $T_{col}(E)$ denotes the transmittance of detector's collimator, and $A(E)$ describes the absorption of x rays in the detector sensitive volume. These transmittance and absorption factors are expressed as follows:

$$T(E) = \exp(-\mu_{\mathrm{Be}}x_{\mathrm{Be}} - \mu_{\mathrm{Au}}x_{\mathrm{Au}} - \mu_{\mathrm{Si}}x_{dead\ layer}), \tag{8}$$

$$T_{col}(E) = \eta\left[1 + \frac{1-\eta}{\eta}\exp(-\mu_{collimator}x_{collimator})\right], \tag{9}$$

$$A(E) = 1 - \exp(-\tau_{\mathrm{Si}}x_{detector}), \tag{10}$$

where μ's are the total x-ray mass attenuation coefficients, τ is the photoelectric absorption mass attenuation coefficient, x's are the mass thickness values of layers determined by the indices, $x_{detector}$ and $x_{collimator}$ are the mass thickness values of detector sensitive layer and collimator, respectively, and η denotes the ratio of the open and full areas of the collimator. In this paper, the detector's collimator is not used. The thickness parameters for the detector used in our experiment, i.e., Be window, Au contact layer, Si dead layer, and detector sensitive layer, were given by the detector manufacturer; these thickness parameters are 12.7 μm for Be window, 38.6 μg/cm^2 for Au contact layer, 0.1 μm for Si dead layer, and 4.21 mm for detector sensitive layer. Based on the model of Eq. (7) and the thickness parameters given by the detector manufacturer, the detection efficiency curve is calculated and also shown in Fig. 2. Moreover, based on the model of Eq. (7) and the experimental detection efficiency curve, these detector thickness parameters are also determined by a nonlinear least-squares fit [52]. The thickness parameters of Be window, Au contact layer, and Si dead layer are obtained by fitting the detector efficiency values in the low-energy region and the detector sensitive layer value is obtained by fitting the detector efficiency values in the high-energy region from the ^{241}Am and ^{137}Cs standard x-ray sources. They are fitted to be 15.01 ± 0.28 μm for Be window, 57.70 ± 6.00 μg/cm^2 for Au contact layer, 0.15 ± 0.03 μm for Si dead layer, and 2.96 ± 0.11 mm for detector sensitive layer. It can be seen that these thickness parameters are acceptable in comparison with that provided by the detector manufacturer. In the calculations above, the total and photoelectric absorption mass attenuation coefficients are taken from the database of the PENELOPE code [44]. The fitted detection efficiency curve is also shown in Fig. 2.

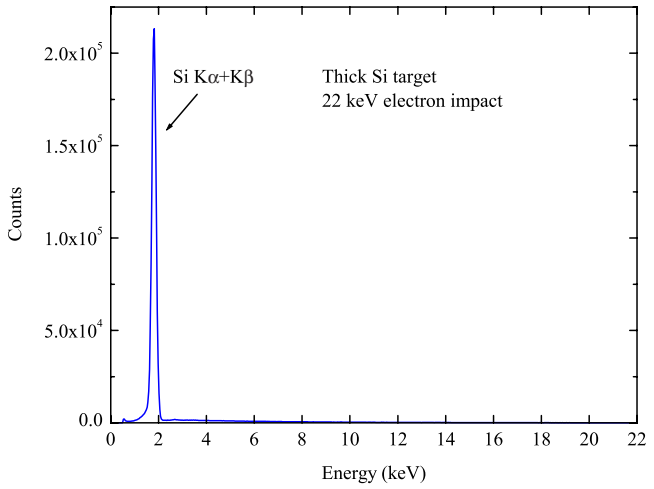

FIG. 3. (Color online) The experimental x-ray spectrum for the thick Si target by 22 keV electron impact.

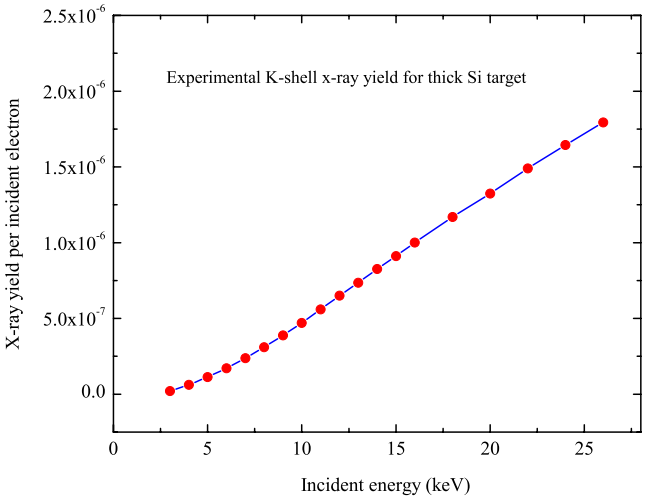

FIG. 4. (Color online) The experimental *K*-shell x-ray yields by electron impact for the thick Si target, $N_X(E_0)/I_0$. The incident electron beam impacts vertically, the x-ray detector is placed horizontally, and the thick Si target is tilted by 45° with respect to the direction of incident electron beam.

III. EXPERIMENTS AND RESULTS

In this paper, the experimental setup is the same as that in [15], i.e., the monoenergetic electron beams from near threshold to several ten keV were provided by an electron gun, and the beam current intensities were adjusted in accordance with characteristic x-ray counting rates. The electron beam current, which impacts on the mirror surface of the thick Si target, was collected by a deep Faraday cup and was fed into an ORTEC digital current integrator, which has an accuracy of less than 1% for the charge measurements. The incident electron beam impacted vertically, the x-ray detector was placed horizontally, and the thick Si target was tilted by 45° with respect to the direction of incident electron beam. The characteristic x rays emitted from the thick Si target were recorded by a Si(Li) x-ray detector with an energy resolution (full width at half maximum) of 190 eV for ^{55}Mn 5.9 keV $K\alpha$ x rays. A typical experimental x-ray spectrum is shown in Fig. 3. The detection efficiency calibration of the Si(Li) detector was performed by the method described in Sec. II C. For the case of the thick Si target, we also performed the Monte Carlo simulations by using the PENELOPE code to estimate the ratios of the incident electrons and secondary electrons which escape from the deep Faraday cup and found that the electron escape ratios from the deep Faraday cup at the incident energy region of interest here are ~3%. The experimental $K\alpha$ and $K\beta$ x-ray yields for the Si thick target, $N_X(E_0)/I_0$, are shown in Fig. 4.

Because the energies of characteristic $K\alpha$ and $K\beta$ x rays of Si element are very close, i.e., 1.74 and 1.84 keV, and cannot be separated in experimental x-ray energy spectra, therefore, in the data processing, Eq. (4) should be modified as follows:

$$K(E,E_0) = \frac{N_A}{A}\left[F_\alpha\left(\frac{\Omega}{4\pi}\varepsilon_\alpha\right)\exp\left(-\mu_\alpha\frac{\cos\alpha}{\cos\beta}\int_E^{E_0}\frac{dE^*}{S(E^*)}\right) + (1-F_\alpha)\left(\frac{\Omega}{4\pi}\varepsilon_\beta\right)\exp\left(-\mu_\beta\frac{\cos\alpha}{\cos\beta}\times\int_E^{E_0}\frac{dE^*}{S(E^*)}\right)\right] \Big/ S(E), \quad (11)$$

where F_α denotes the $K\alpha$ x-ray emission rate, $\Omega\varepsilon_\alpha/4\pi$ and $\Omega\varepsilon_\beta/4\pi$ represent the detection efficiencies at the energies of $K\alpha$ and $K\beta$ x rays of Si element, and μ_α and μ_β are the mass attenuation coefficients for $K\alpha$ and $K\beta$ x rays of Si element inside the Si thick target. The $K\alpha$ x-ray emission rate, F_α, is derived from the most probable value of $K\beta$ to $K\alpha$ x-ray intensity ratio for Si element [56], which is 0.9756. The detection efficiencies at the energies of $K\alpha$ and $K\beta$ x rays of Si element, $\Omega\varepsilon_\alpha/4\pi$ and $\Omega\varepsilon_\beta/4\pi$, are obtained by interpolating the fitted detection efficiency curve; they are 1.7408×10^{-4} and 1.7838×10^{-4}. The *K*-shell fluorescence yield for Si element is taken from the recommended value of Hubbell *et al.* [57], i.e., 0.043. The mass attenuation coefficients, μ_α and μ_β, for $K\alpha$ and $K\beta$ x rays of Si element inside the Si thick target are calculated from the XCOM code [58]; they are 359.1 and 310.6 cm^2/g, respectively. The mass stopping powers, $S(E)$, are taken from the database of the PENELOPE code [44]. The *K*-shell ionization threshold energy for Si element is 1.8389 keV.

Finally, the *K*-shell ionization cross sections for Si element in the energy region of 3–25 keV are experimentally obtained by the thick-target method described in Sec. II, and the code FTIKREG [43] is used to implement the Tikhonov regularization method. The experimental results are shown in Fig. 5 and given in Table I. The error estimation of the thick-target method has been given in [41]. In this paper for the case of the thick Si target, the main error sources include the error from the statistical error of net peak counts (~1%), the errors of the detection efficiency calibration (~5%), the *K*-shell fluorescence yield (~10%), the escape of incident electrons (~3%), the error originated from the mass attenuation coefficient and the mass stopping power (~5%) [41], and the error of numerical method from the Tikhonov regularization (~5%) [41]; therefore, the estimated total error, obtained by combining all errors indicated above in quadrature, is ~13%. In Fig. 5, the experimental *K*-shell ionization cross sections for Si element obtained in this paper are com-

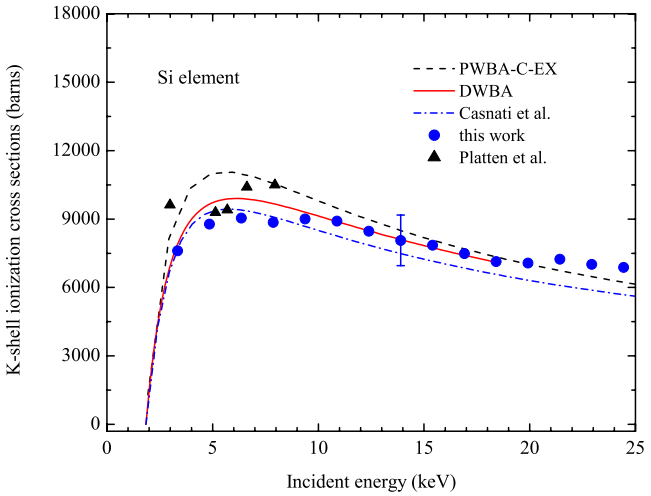

FIG. 5. (Color online) The experimental *K*-shell ionization cross sections for Si element obtained in this paper (circles) are compared with the theoretical values based on the DWBA model developed by Segui and co-workers [28,59] (solid line). The theoretical values based on the PWBA-C-Ex model [20,60] (dashed line) and the empirical formula of Casnati *et al.* [31] (dash dot line) are also shown. The triangles indicate the experimental values of Platten *et al.* [61].

pared with the theoretical values based on the DWBA model developed by Segui and co-workers [28,59]. The theoretical values based on the PWBA-C-Ex model [20,60] and the empirical formula of Casnati *et al.* [31] are also shown in Fig. 5. From Fig. 5, we can see that the theoretical values of both the DWBA model of Segui and co-workers [28,59] and of the empirical formula of Casnati *et al.* [31] are similar and they are in good agreement with the experimental data obtained in this paper. Moreover, on the whole, the theoretical values of the PWBA-C-Ex model [20,60] are higher than our experimental data in the lower-energy region. In addition, the experimental data for Si element near the threshold energy region available in the literature are also plotted in Fig. 5 [9,61].

IV. CONCLUSIONS

In this paper, the *K*-shell ionization cross sections of Si element near the threshold energy region have been measured by using the thick-target method. The effects of multiple scattering of incident electrons and from the bremsstrahlung photons and other secondary particles have been discussed using the Monte Carlo simulations. The detection efficiency calibration in the lower-energy region has been performed by using the bremsstrahlung spectra of thick carbon target by electron impact in combination with the use of standard x-ray sources, and the detector thickness parameters have also been determined by a nonlinear least-squares fit to the experimental detection efficiency curve. The Tikhonov regularization method has been utilized to deal with the ill-posed inverse problem involved in the thick-target method. These experimental data obtained in this paper have also been compared with some theoretical models and empirical formula, and it has been observed that the experimental data in this paper are in good agreement with the DWBA model developed most recently.

TABLE I. The experimental *K*-shell ionization cross sections for Si element obtained in this paper.

Energy (keV)	Cross sections (barn)	Errors (barn)
3.35	7612	1033
4.85	8777	1191
6.36	9043	1228
7.87	8858	1205
9.37	9007	1227
10.88	8915	1216
12.39	8468	1158
13.89	8067	1106
15.40	7853	1077
16.91	7489	1030
18.41	7138	984
19.92	7072	978
21.43	7246	1002
22.93	7019	974
24.44	6880	956

ACKNOWLEDGMENTS

Financial support from the National Natural Science Foundation of China (Grant Nos. 10674097 and 10774106), the Program for New Century Excellent Talents in University (Grant No. NCET-05-0780), and the International Atomic Energy Agency (Grant No. 13491/R3) are gratefully acknowledged.

[1] C. J. Powell, Rev. Mod. Phys. **48**, 33 (1976).
[2] C. J. Powell, in *Electron Impact Ionization*, edited by T. D. Märk and G. H. Dunn (Springer-Verlag, New York, 1985), Chap. 6, pp. 198–231.
[3] H. Schneider, I. Tobehn, F. Ebel, and R. Hippler, Phys. Rev. Lett. **71**, 2707 (1993).
[4] Y. Nagashima, F. Saito, Y. Itoh, A. Goto, and T. Hyodo, Phys. Rev. Lett. **92**, 223201 (2004); **92**, 239902(E) (2004).
[5] F. Salvat, X. Llovet, J. M. Fernández-Varea, and J. Sempau, Microchim. Acta **155**, 67 (2006).
[6] D. Salzmann, Ch. Reich, I. Uschmann, E. Förster, and P. Gibbon, Phys. Rev. E **65**, 036402 (2002).
[7] D. Riley, J. J. Angulo-Gareta, F. Y. Khattak, M. J. Lamb, P. S. Foster, E. J. Divall, C. J. Hooker, A. J. Langley, R. J. Clarke, and D. Neely, Phys. Rev. E **71**, 016406 (2005).
[8] P. Köster, K. Akli, D. Batani, S. Baton, R. G. Evans, A. Giuli-

etti, D. Giulietti, L. A. Gizzi, J. S. Green, M. Koenig, L. Labate, A. Morace, P. Norreys, F. Perez, J. Waugh, N. Woolsey, and K. L. Lancaster, Plasma Phys. Controlled Fusion **51**, 014007 (2009).
[9] M. T. Liu, Z. An, C. H. Tang, Z. M. Luo, X. F. Peng, and X. G. Long, At. Data Nucl. Data Tables **76**, 213 (2000).
[10] X. Llovet, C. Merlet, and F. Salvat, J. Phys. B **33**, 3761 (2000).
[11] C. S. Campos, M. A. Z. Vasconcellos, X. Llovet, and F. Salvat, Phys. Rev. A **66**, 012719 (2002).
[12] C. Merlet, X. Llovet, and J. M. Fernández-Varea, Phys. Rev. A **73**, 062719 (2006); **74**, 049901(E) (2006).
[13] Z. An, T. H. Li, L. M. Wang, X. Y. Xia, and Z. M. Luo, Phys. Rev. A **54**, 3067 (1996).
[14] Z. An, C. H. Tang, C. G. Zhou, and Z. M. Luo, J. Phys. B **33**, 3677 (2000).
[15] Y. Wu, Z. An, Y. M. Duan, M. T. Liu, and C. H. Tang, J. Phys. B **40**, 735 (2007).
[16] R. K. Singh and R. Shanker, J. Phys. B **36**, 3031 (2003).
[17] C. Merlet, X. Llovet, and F. Salvat, Phys. Rev. A **78**, 022704 (2008).
[18] Y. Nagashima, W. Shigeta, T. Hyodo, and M. Iwaki, Radiat. Phys. Chem. **76**, 465 (2007).
[19] M. Dingfelder, S. Segui, and J. M. Fernández-Varea, Phys. Rev. A **77**, 062710 (2008).
[20] R. Hippler, Phys. Lett. A **144**, 81 (1990).
[21] P. Rez, J. Res. Natl. Inst. Stand. Technol. **107**, 487 (2002).
[22] J. P. Santos, F. Parente, and Y.-K. Kim, J. Phys. B **36**, 4211 (2003).
[23] Y.-K. Kim, J. P. Santos, and F. Parente, Phys. Rev. A **62**, 052710 (2000).
[24] M. A. Uddin, A. K. F. Haque, M. M. Billah, A. K. Basak, K. R. Karim, and B. C. Saha, Phys. Rev. A **71**, 032715 (2005).
[25] M. A. Uddin, M. A. K. Fazlul Haque, A. K. Basak, and B. C. Saha, Phys. Rev. A **70**, 032706 (2004).
[26] A. I. Mikhailov, A. V. Nefiodov, and G. Plunien, Phys. Lett. A **372**, 4451 (2008).
[27] A. I. Mikhailov, A. V. Nefiodov, and G. Plunien, Phys. Lett. A **372**, 5171 (2008).
[28] S. Segui, M. Dingfelder, and F. Salvat, Phys. Rev. A **67**, 062710 (2003).
[29] J. Colgan, C. J. Fontes, and H. L. Zhang, Phys. Rev. A **73**, 062711 (2006).
[30] D. Bote and F. Salvat, Phys. Rev. A **77**, 042701 (2008).
[31] E. Casnati, A. Tartari, and C. Baraldi, J. Phys. B **15**, 155 (1982); **16**, 505 (1983).
[32] C. Hombourger, J. Phys. B **31**, 3693 (1998).
[33] C. H. Tang, Z. An, X. Q. Fan, and Z. M. Luo, Chin. Phys. Lett. **18**, 1053 (2001).
[34] A. K. F. Haque, M. A. Uddin, A. K. Basak, K. R. Karim, and B. C. Saha, Phys. Rev. A **73**, 012708 (2006).
[35] A. K. F. Haque, M. A. Uddin, A. K. Basak, K. R. Karim, B. C. Saha, and F. B. Malik, Phys. Rev. A **73**, 052703 (2006).
[36] C. Merlet, X. Llovet, and F. Salvat, Phys. Rev. A **69**, 032708 (2004).
[37] Z. An, M. T. Liu, Y. C. Fu, Z. M. Luo, C. H. Tang, C. M. Li, B. H. Zhang, and Y. J. Tang, Nucl. Instrum. Methods Phys. Res. B **207**, 268 (2003).
[38] M. P. Seah *et al.*, Surf. Interface Anal. **36**, 1269 (2004).
[39] Z. An, Y. Wu, M. T. Liu, Y. M. Duan, and C. H. Tang, Nucl. Instrum. Methods Phys. Res. B **246**, 281 (2006).
[40] L. X. Tian and Z. An, Nucl. Instrum. Methods Phys. Res. B **266**, 5037 (2008).
[41] Z. An and Q. Hou, Phys. Rev. A **77**, 042702 (2008).
[42] C. Elster, J. Honerkamp, and J. Weese, Rheol. Acta **30**, 161 (1991).
[43] J. Weese, Comput. Phys. Commun. **69**, 99 (1992).
[44] F. Salvat, J. M. Fernández-Varea, E. Acosta, and J. Sempau, PENELOPE (Version 2002-b), A Code System for Monte Carlo Simulation of Electron and Photon Transport, NEA/NSC/DOC, Pairs, 2001, 19.
[45] E. Acosta, X. Llovet, and F. Salvat, Appl. Phys. Lett. **80**, 3228 (2002).
[46] X. Llovet, L. Sorbier, C. S. Campos, E. Acosta, and F. Salvat, J. Appl. Phys. **93**, 3844 (2003).
[47] J. Sempau, J. M. Fernández-Varea, E. Acosta, and F. Salvat, Nucl. Instrum. Methods Phys. Res. B **207**, 107 (2003).
[48] Z. An and M. T. Liu, Nucl. Instrum. Methods Phys. Res. B **194**, 513 (2002).
[49] S. M. Seltzer and M. J. Berger, Nucl. Instrum. Methods Phys. Res. B **12**, 95 (1985).
[50] S. M. Seltzer and M. J. Berger, At. Data Nucl. Data Tables **35**, 345 (1986).
[51] L. Kissel, C. A. Quarles, and R. H. Pratt, At. Data Nucl. Data Tables **28**, 381 (1983).
[52] Z. An, M. T. Liu, Y. Wu, and Y. M. Duan, At. Energy Sci. Technol. **40**, 83 (2006) (in Chinese).
[53] M.-M. Bé, V. Chisté, C. Dulieu *et al.*, International Atomic Energy Agency, Vienna, December, 2005 (http://www-nds.iaea.org/xgamma_standards/).
[54] W. J. Gallagher and S. J. Cipolla, Nucl. Instrum. Methods **122**, 405 (1974).
[55] I. Uzonyi, Gy. Szabó, I. Borbély-Kiss, and Á. Z. Kiss, Nucl. Instrum. Methods Phys. Res. B **210**, 147 (2003).
[56] Md. R. Khan and M. Karimi, X-Ray Spectrom. **9**, 32 (1980).
[57] J. H. Hubbell, P. N. Trehan, N. Singh, B. Chand, D. Mehta, M. L. Garg, R. R. Garg, S. Singh, and S. Puri, J. Phys. Chem. Ref. Data **23**, 339 (1994).
[58] M. J. Berger, J. H. Hubbell, S. M. Seltzer, J. Chang, J. S. Coursey, R. Sukumar, and D. S. Zucker, XCOM, Photon Cross Section Database (Version 1.3), National Institute of Standards and Technology, Gaithersburg, MD, 2005 (http://physics.nist.gov/xcom); originally published by M. J. Berger and J. H. Hubbell, XCOM, Photon Cross Sections on a Personal Computer, NBSIR 87–3597, National Bureau of Standards (former name of NIST), Gaithersburg, MD, 1987.
[59] C. S. Campos, M. A. Z. Vasconcellos, J. C. Trincavelli, and S. Segui, J. Phys. B **40**, 3835 (2007).
[60] Z. An, Z. M. Luo, and C. H. Tang, Nucl. Instrum. Methods Phys. Res. B **179**, 334 (2001).
[61] H. Platten, G. Schiwietz, and G. Nolte, Phys. Lett. **107A**, 83 (1985).